Journal of Advanced Research in Applied Sciences and Engineering Technology

Journal homepage:
https://semarakilmu.com.my/journals/index.php/applied_sciences_eng_tech/index
ISSN: 2462-1943

Immersion Time Dependence in the Fabrication of Cesium Bismuth Iodide ($Cs_3Bi_2I_9$) Perovskite Solar Cells (PeSCs) by the Hot Immersion Method

Mohd Faizal Achoi[1,*], Muhamad Haziq Zulkeflee[2], Shinya Kato[2], Naoki Kishi[2], Tetsuo Soga[2]

[1] Faculty of Applied Sciences, Universiti Teknologi MARA, Cawangan Sabah, Kampus Kota Kinabalu, 88997 Kota Kinabalu, Sabah, Malaysia
[2] Department of Electrical and Mechanical Engineering, Nagoya Institute of Technology, Gokiso-cho, Showa-ku, Nagoya, 466-8555 Aichi, Japan

ARTICLE INFO

Article history:
Received 10 February 2026
Received in revised form 30 May 2026
Accepted 2 June 2026
Available online 14 August 2026

Keywords:
CBI; Immersion time; Perovskite; Solar cells; Hot immersion method

ABSTRACT

Up to date, lead (Pb)-based perovskite solar cells (PeSCs) were widely discovered due to its outstanding performance, however, it is a toxic and unstable material, while the Cesium (Cs)-based PeSCs is a non-toxic and stable material. In this paper, the hot immersion time (HIT) dependence in the fabrication of cesium bismuth iodide ($Cs_3Bi_2I_9$-CBI) PeSCs fabricated through the hot immersion method (HIM) is reported. The CBI fabricated using a simple method by changing the hot immersion time between 1 h and 24 h. The XRD results showed that the crystallinity of the CBI film was improved, while the surface morphology showed that the compact and dense film were enhanced. On increasing the HIT, an increase in the average thickness film from 0.918 µm to 4.22 µm was observed. The increase in the thickness led to an extension of band-edge absorption region of CBI film, which is the absorption band-edge region at 647 nm that is extended to 678 nm wavelength with a narrower indirect bandgap, which is from 1.81 eV to 1.65 eV. Consequently, high light absorption of CBI cell due to the high surface roughness, which is 42.33 x 10^2 nm at 18 h attributed to a better light trap and hence reduced the light reflection effect on the CBI film surface. Eventually, the performance of HIM-fabricated CBI-PeSCs showed an increment, particularly the short-circuit current density (J_{sc}), which is fourfold increases, i.e., from 3.0 x 10^{-2} mA/cm^2 to 0.11 mA/cm^2, while the open-circuit voltage showed fifteenfold increases, i.e., from 0.008 V to 0.12 V, at 18 h of hot immersion time. Our finding suggests that by using HIM, the electronic properties of CBI-PeSCs are still attainable through a simple method and it can be improved by HIT. Yet providing a low-cost approach for the fabrication of Pb-free PeSCs in future work.

1. Introduction

Recently, lead-(Pb) based perovskite solar cells (PeSCs) have been attracted much attention by previous researchers due to their outstanding properties such as high efficiency and abundant material [1,2]. However, Pb-PeSCs faced problems with toxic and stability issues. For example, UV radiation from the sunlight distorted the Pb-PeSCs in ambient air and it caused the degradation as reported by Lee *et al*., [3]. In addition, lead in $CH_3NH_3PbI_3$ (MA_3PbI_3-ABX_3) perovskite material made them environmentally unfriendly, and thus limited the commercialization of halide perovskite-based

* *Corresponding author.*
E-mail address: mohdf484@uitm.edu.my

materials [4]. Currently, researchers unlock other potential of perovskite material, for example Sn and Ge-based perovskite material, however, they are suffering toxicity and inconsistencies of structural. Furthermore, the researchers focused on enhancing stability and minimizing toxicity of perovskite materials. At the same time, searching for the right candidate to replace the Pb-based PeSCs. Therefore, among metal cation (B) have been considerable interest in ABX_3 (A = MA^+, FA^+, Cs^+, B= Pb, Bi, X = Cl, Br, I) form of perovskite structure, are Bi^{3+}, Sn^{2+}, Ge^{2+} and Sb^{3+}. They form a Pb-free perovskite compound with a halide group, such as F^-, Cl^-, Br^-, and I^-. It means that they replace Pb in ABX_3 perovskite compound structure with Bi^{3+} or Cs^+ to form $[BX_3]$ octahedra structure with halogen groups called as a Pb-free perovskite compounds, whereas the example of A in ABX_3 is organic compounds, such as methylammonium cation ($CH_3NH_3^+$; MA^+), formamidinium cation ($HC(NH_2)_2)^+$; FA^+) and others. Herein, we are selecting the A is Cesium (Cs^+) which is monovalent of metal cation. The reason for this selection is that the stability of Cs^+ in ambient air for long term periods compared to organic cations (MA^+ and FA^+) have tendency to degrade in the long-term period. M. Kulbak *et al*., who reported Cs based perovskite solar cell has shown excellent thermal stability [5], while Pb in ABX_3 will be replaced with the Bi^{3+} due to the stability and non-toxic element compared to Pb. According to M. Lyu *et al.*, who reported the bismuth-based perovskite is a non-toxic and stable element [6]. It means that the bismuth has electron valence of $6s^2$ made its stable element, moreover, Pb and Bi have similar electron configuration [7]. Eventually, the Pb-free perovskite compound formed, which is cesium bismuth iodide [$Cs_3Bi_2I_9$ (ABX_3)]-based PeSCs that will be fabricated through a newly developed method called hot immersion method (HIM) and it will be further discussed in the next two paragraphs.

In this connection, among the criteria of ideal properties of Pb-free perovskite materials are non-toxic material, stable in ambient air, a narrow bandgap, high optical absorption coefficients, higher mobilities and long-term stability [8]. In respective of those characteristics made the perovskite materials suitable in the application of optoelectronics device, and photovoltaic [9]. They also show remarkable performance in the field of solar cell application and electronic devices such as lasers, light-emitting diodes and memristors [4]. In general, $Cs_3Bi_2I_9$ (ABX_3) based perovskite solar cells have shown eco-friendly, stable compound and non-toxic materials [10]. In addition, Cs^+ cation has good optical properties, whereby it capable of changing the light absorption of perovskite material and it might be attributed to the device's performance [11]. Likewise, Bi^{3+} is a non-toxic element [6] and high carrier mobility [12], which may be beneficial for the CBI-PeSCs performance.

On the other hand, CBI films have been fabricated mostly by spin-coating and using DMF or DMSO as a solvent in the CsI precursor solution preparation [13]. However, this method has limited space to grow $Cs_3Bi_2I_9$ single crystals [14,15,16]. Corresponding to that, spin-coating requires nitrogen gas to perform the deposition process, while it's wasting the precursor solution. In addition, the spray-coating techniques, reported by S. Devasia *et al*., are still suffering issues with the CBI film morphological [13]. Similarly, Md. Shahiduzzaman *et al*., who is employed vacuum-deposited to deposit the CBI thin film suffered a non-compact film [8]. Moreover, those methods required technical handling and needed controlling parameters such as the parameters of gas pressure level, vacuum condition, employing gas, spinning speed and the time of coating [4]. Other methods in the same manner problems are chemical vapor deposition [17], dripping of solvent [18], and MA gas deposition [19].

Hence, in this study, we employ a simple method at low-temperature processing, less controlling parameters and does not require technical handling [7] to fabricate the CBI-PeSCs. According to our previous studies [20], hot immersion method (HIM) is a promising method to fabricate Pb-free perovskite film with high crystallinity, compact film and a narrower optical bandgap [20,21,22]. In addition, this method has shown the suitability and in situ formation of CBI thin film with a compact,

dense film, pinhole-free and high crystallinity as reported in our recent studies [7]. Herein, the influence of immersion times in the fabrication of CBI-film and its properties are evaluated. The immerse fabricated CBI-PeSCs performance is evaluated as well. To the best of our knowledge, the immersion time dependence in the fabrication of CBI-PeSCs has not been reported elsewhere, particularly using hot immersion method (HIM). Correspondingly, the knowledge gap of this study with other reports in terms of CBI and its performance is the HIM have been employed with varying of immersion times, particularly involving Pb-free perovskite compound. In addition, the electronic properties of CBI cells such as current density and voltage have been enhanced by using this simple method compared to previous reports [7,18].

In summary, by optimizing the influence of immersion time, the CBI film with high crystallinity and roughness surface, compact and pinhole-free film have been successfully fabricated by a simple method in this study. In addition, the optical properties of CBI-PeSCs have shown a remarkable improvement, particularly the optical bandgap compared to previous studies [4,7,23] and the light absorption properties are still attainable at high absorbance intensity. Consequently, the CBI cell performance is still managed to be achievable, even though the performance of CBI-PeSCs is still low at present. There are some advantages that can be explored furthermore through HIM, and it gives some hint that using HIM gives a promising way to fabricate high-crystalline, compact, pinhole-free and narrower bandgap of Pb-free perovskite. At the same time, this study was useful and gave an idea in a new way and simple approach to fabricate CBI film and it thus contributed to the body of knowledge for the development of Pb-free PeSCs in future.

2. Methodology

2.1 Experimental

Firstly, the preparation of fluorine tin oxide (FTO) substrate and the fabrication of poly(3-hexylthiophene-2,5-diyl) P3HT as hole transport layer (HTL), compact and mesoporous titanium dioxide (mp-TiO_2) as an electron transport layer (ETL) are referred to ref. [36]. Next, the precursor of $Cs_3Bi_2I_9$ (CBI) was prepared, where the preparation of CBI, precursor of cesium iodide (CsI) and bismuth triiodide (BiI_3) (both purchased from Sigma-Aldrich, 99.999%) were mixed with ratio [1.5:1.0] in 10 mL of dimethyl formamide [$HCON(CH_3)_2$] (DMF) as a solvent, to form a 0.5 M CBI solution. The mixture was then continuously stirred for 1 h at 60 ^oC to allow the solution mixed vigorously and it left for aging time. The solution is then ready for immersion deposition, in which the sample of mp-TiO_2/c-TiO_2/FTO/glass immersed in 0.5 M of CBI solution at 30 ^oC for 1 h as shown in inset Figure 5(i). The reason for selection of hot immersion temperature at 30 ^oC is to ensure the immersion solution does not evaporate at high temperature. O. Shargaieva *et al*., reported high temperatures may cause the evaporation of the solution [24]. All these steps are repeated for the preparation of different immersion times of CBI solution, which are 6 h, 12 h, 18 h, and 24 h, according to the previous reported work [25]. Next, the annealing of CBI/mp-TiO_2/c-TiO_2/FTO/glass at 100 ^oC for 10 min and the sample left for cooling in the room temperature. Finally, the fabrication of poly(3-hexylthiophene-2,5-diyl) (P3HT) as a Hole Transport Layer (HTL) and carbon electrode is referred to [26] and followed by the silver paste on the carbon layer, and dried in room temperature for 5 min. In brief, P3HT powder was dissolved in dichlorobenzene to make 15 $mg.mL^{-1}$ of P3HT and then followed by P3HT solution was spin-coated at 5000 rpm for 30 s. The sample is then annealed on a hot plate at 150 ^oC for 10 min. The whole fabrication process was carried out in a dry nitrogen-filled glovebox except for the silver paste and carbon colloidal deposition. The purpose of using the carbon was to provide a better connection between the connector (Ag paste) and the entire CBI cell structure

[27] as shown in inset Figure 5(i). Note that the fabrication of CBI films was fabricated three samples for each of immersion times to ensure the reproducibility of the sample.

2.2 Characterization

The structural and morphology of CBI films were characterized by X-ray diffractometer (XRD) (Rigaku RINT-2100 diffractometer) with the radiation source of Ni-filtered Cu Kα radiation with wavelength, λ = 1.5408 Å and equipped with a Cu target (Rigaku Smartlab) and scanning electron microscopy (SEM) (JEOL JSM-7600F), respectively, while the optical properties of CBI film and the CBI-PeSCs performance were characterized using UV-vis spectrophotometer (JASCO Model V-570) and the solar simulator under simulated solar white light illumination at AM 1.5, 100 $mW.cm^{-2}$, respectively. Finally, the thickness of a film was measured using the Dektak measurement (Veeco-Dektak 150).

3. Results

3.1 Structural properties

Figure 1 shows the XRD curves of CBI-PeSCs for different hot immersion times (HIT). The crystallite structure of $Cs_3Bi_2I_9$ (CBI) exhibit the hexagonal structure ($P6_3/mmc$) and have a zero-dimensional structure with isolated bioctahedrons [28]. Our XRD pattern is well matched with the recently reported results [29]. All the XRD patterns are indexed as a hexagonal $Cs_3Bi_2I_9$ (JCPDS No. 23-0847) [28-32]. The deposited CBI films show six typical diffraction peaks at 2θ = 12.82°, 25.86°, 27.54°, 29.68°, 32.40°, and 42.92° [7], which are assigned to (101), (006), (202), (203), (204) and (0010) lattice plane, respectively. Other CBI peaks are observed at diffraction angles of 21.22°, 24.84° and 45.79° [33,[34]. At 1 h of immersion time, seven peaks of CBI are seen as low in intensity except for the peak at 25.86°, which appears as a narrow and intense peak. By increasing the immersion time to 6 h, the CBI peak starts to increase in intensity, as can be seen at 12.83°, 27.54°, 29.68° and 32.40°, and now eight peaks of CBI appeared as compared to what seen earlier. At the same time, one new peak of CBI starts to appear at 21.22°, while other CBI peaks remain the same as before. It means that the crystallinity of deposited CBI film starts to increase. As for further increasing the immersion time to 12 h, now nine CBI peaks appeared as can be seen in Figure 1(c), with one new peak of CBI appears at 37.80°, and at the same time, the CBI peaks at 25.86° and 27.54° are further gradually increased, while other CBI peaks start to a bit decrease in intensity. However, on prolonging the immersion time to 18 h, interestingly more peaks of CBI have appeared with twelfth peaks compared to what seen before, whereas the intensity of CBI peaks further increases as well, particularly the CBI peaks at 25.86° and 42.92°, and at the same time, two new peaks of CBI start to appear at 24.84° and 45.86°. It means that the crystallinity of the CBI films is being further enhanced. Finally, at 24 h of immersion time, now six peaks of CBI left as compared to seen earlier, with six peaks of CBI disappeared while another six peaks remain with low in intensity at 12.82°, 29.68°, and 42.92°, except for the CBI peaks at 25.86° remain the same. It indicates that the crystallinity of CBI films was become poor at longer time of immersion, and this might be probably due to the evaporation of the solvent [24]. In brief, in a short time of immersion, only a few peaks appeared, and all the CBI peaks were low in intensity, whereas, in a longer time of immersion it can be observed that more peaks of CBI appeared with narrow peaks and high in intensity. The XRD results elucidate that improved crystallinity has a relationship with the surface morphology of CBI, which will be discussed in the next section.

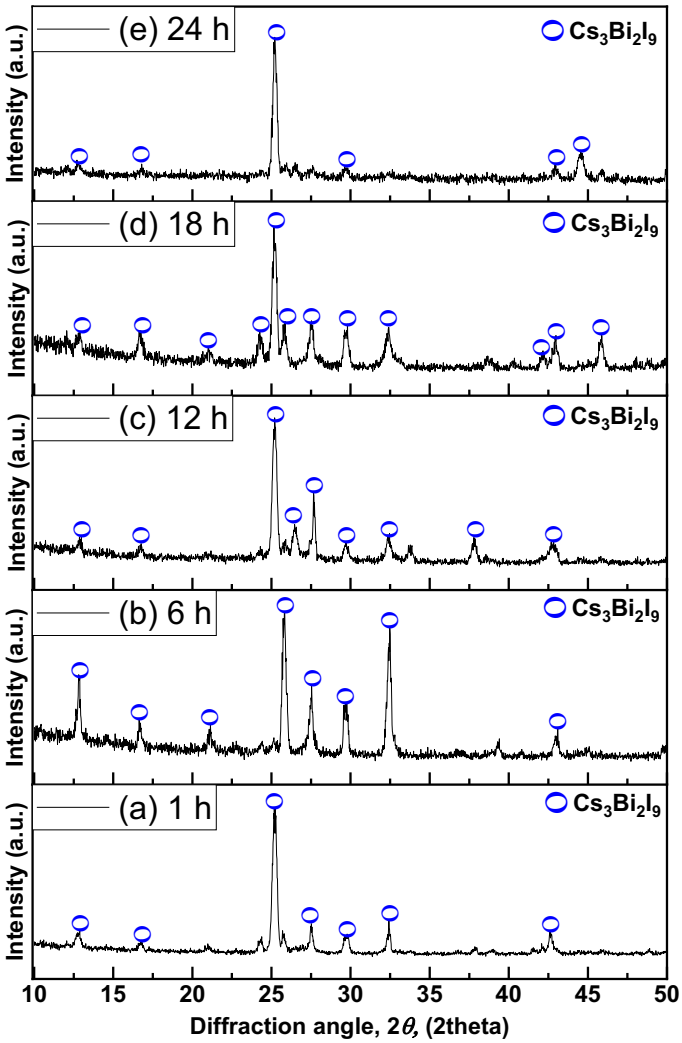

Fig. 1. XRD curves of CBI films at different immersion times: (a) 1 h, (b) 6 h, (c) 12 h, (d) 18 h and (e) 24 h

3.2 Surface morphology properties

Figure 2 visually depicts the SEM morphologies of the CBI films at different immersion times. At 1 h of immersion time, it can be observed that non-smooth surface and non-uniform film of CBI, as confirmed by the XRD result in Figure 1(a), resulting in a rougher surface of 17.53 x 10^2 nm that measured by the Dektak measurement as shown in Figure 3(a). This happened might be due to the CBI structure itself has hexagonal structure [35] with large size attributed to rougher surface. In addition, the CBI solution does not have enough time to crystallize at shorter time of immersion. Consequently, resulted in some defect, which is valley can be seen on the CBI surface as shown in yellow colour. On increasing the immersion times to 6 h, some of the CBI surface starts to being flatted and now the surface roughness of CBI film reduces to 9.18 x 10^2 nm, however, a few of defects are seen on the surface of CBI in denoted of pink colour as shown in Figure 2(b). It means that a few of CBI being crystallize with 30 ^oC of immersion temperature. Further increasing the immersion time to 12 h, as can be seen in SEM images of Figure 2(c), resulted in a very few defects compared to what seen earlier in 6 h and importantly, some of hexagonal CBI shape appeared as indicated in red colour, hence as prove that the CBI start to crystallize at longer time of immersion compared to seen before in 1 h and 6 h, whereby none of CBI hexagonal shape formed at a shorter time, particularly the rectangular shape size of CBI hexagonal side structure is seen randomly distributed and arranged

upwards, while sank with each other as indicated in red colour of Figure 2(c). It means the hexagonal CBI starting to grow largely encouraged by the nucleation growth. Our explanation is in line with our previous findings that reported in [7]. Consequently, the roughness increases back from 9.18 x 10^2 nm to 21.71 x 10^2 nm, which resulted in inhomogeneous and non-flat surface, as shown in Figure 3(a) and Figure 2(c), respectively. On prolonging the HIT to 18 h, interestingly, non-uniform and hexagonal shape edge are out of the surface as seen earlier now became disappeared, combined and sank with each other, and then CBI morphology starts becoming uniform and compact surface, without defect as seen before. This happened due to crystallization process and nucleation growth [7]. The compact surface indicates that the crystallinity of CBI film much enhanced in line with the XRD result as discussed earlier in Figure 1(d). This time, the surface roughness became much improved, from 21.71 x 10^2 nm increased to 42.33 x 10^2 nm, as can be seen in Figure 2(d) and Figure 3(a), respectively. Thus, the rougher surface gave advantage for light trapping with reduced reflection effect, and it expected will influence the performance of CBI solar cells [22], which will be discussed further in CBI-PeSCs performance. Finally, increasing the immersion time to 24 h, surprisingly, it can be seen the CBI surface is now become compact with a less rough surface than before, with the surface roughness, Ra, is 14.38 x 10^2

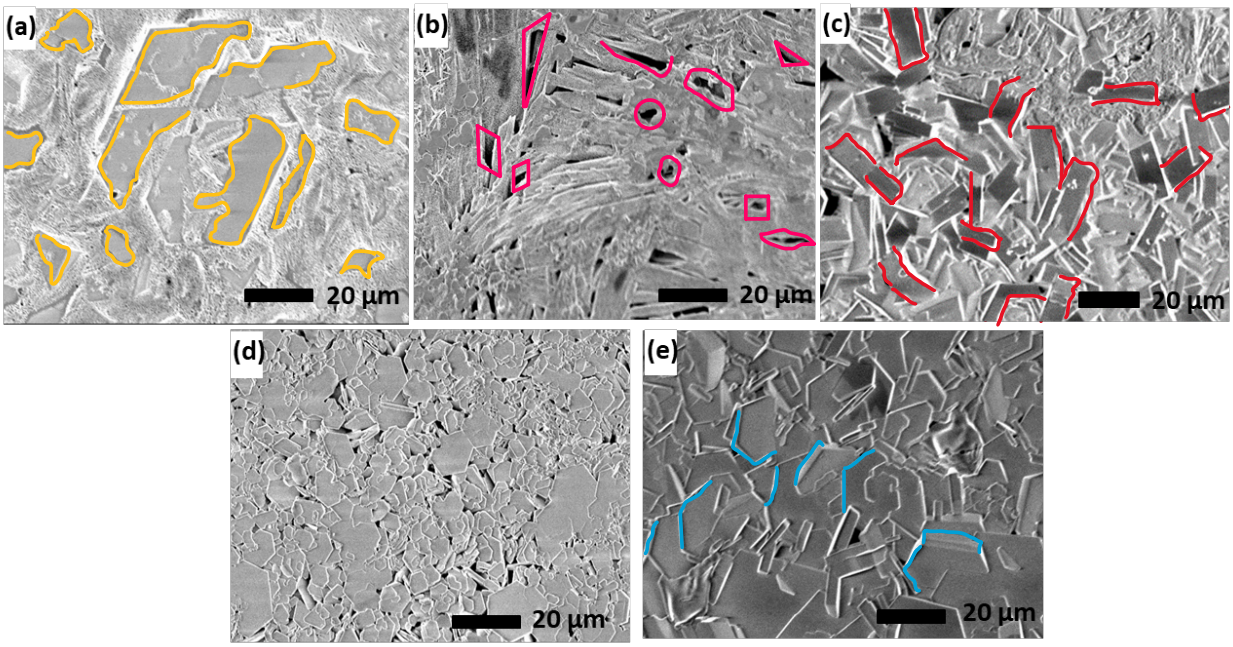

Fig. 2. SEM morphologies of CBI films at different immersion times: (a) 1 h, (b) 6 h, (c) 12 h, (d) 18 h and (e) 24 h

nm, as shown in Figure 3(a) and confirmed by the Dektak measurement. It thus indicates that the CBI film is now become smooth and flat surface resulting in pinhole-free compared to what seen earlier. In addition, the CBI hexagonal shape buried and was sank with each other, as can be seen in blue colour of Figure 2(e), which also attributed to the smoothness and less rough of CBI film as shown in Figure 3(a) of 24 h sample. In brief, the surface roughness has a relationship with the compactness and the homogeneity of an CBI film. The surface roughness associated with the crystallite size will be further discussed on the next paragraph. Correspondingly, the improved morphology and pinhole-free of CBI film is expected to enhance the optical absorption, which will be further discussed either in the UV-Vis Section. In addition, it might be improving the performance of CBI-PeSCs and will be further discussed as well in the PV section.

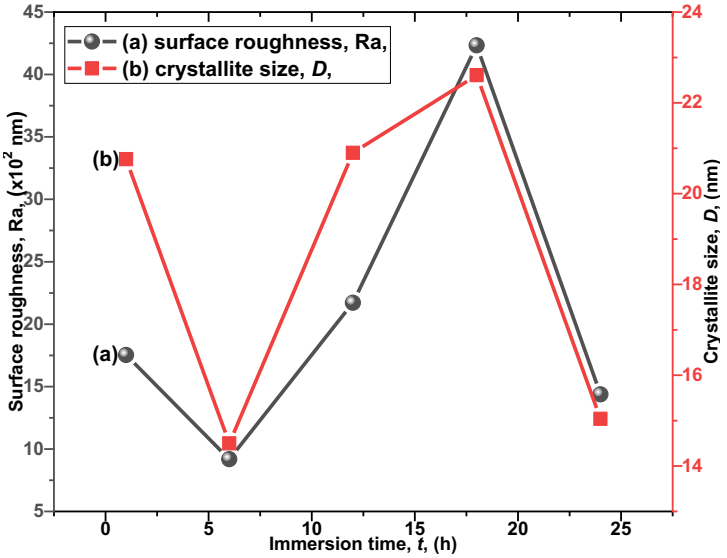

Fig. 3. The relationship of surface roughness (a) and crystallite size (b) of CBI films at different immersion times: (a) 1 h, (b) 6 h, (c) 12 h, (d) 18 h and (e) 24 h

Figure 3 shows the plotted graph of Ra and *D* against time. The crystallite size, *D*, of the CBI film was calculated by using Scherer's equation [31,32]. In general, these two plotted graphs indicate the relationship between two parameters, which is surface roughness and crystallite size against the immersion times of the CBI film. It indicates that as the immersion times increases, the trend of fluctuating accordingly is shown by two parameters. This means the HIT influences the surface roughness and crystallite size of the CBI. In addition, the crystallite size and surface roughness are associated with the CBI film compactness and uniformity, as discussed earlier in Figure 2. In a short time of immersion, 1 h, in Figure 3(a) and 3(b), Ra and *D* are 17.53 x 10^2 nm and 20.76 nm, respectively. However, at a longer time of immersion, 24 h, Ra and *D* are 14.38 x 10^2 nm and 15.04 nm, respectively. This can be elucidating that the immersion times plays crucial role in determining the compactness and uniformity of CBI film in terms of film roughness and crystallite size. At 1 h of immersion time, the Ra and *D* values are higher than 6 h of immersion due to nucleation growth [7,31] and interdiffusion process that does not happen in a short time of immersion [36]. In other word, the CBI crystal structure does not have enough time to crystallize, while the reaction time has not fully completed yet. As a result, it created a valley or defect on the surface of CBI film as can be seen in yellow colour of Figure 2(a). Instead, starts changing of the CBI surface occurred as discussed earlier in SEM section caused the Ra and *D* values are being reduced, whereby 9.18 x 10^2 nm and 14.50 nm, respectively. However, as the nucleation growth and crystallization process happened, in which the CBI crystal structure grow largely caused the CBI hexagonal shape side are out of the surface as discussed earlier in SEM section of Figure 2(c) and now, the Ra and *D* are 21.71 x10^2 nm and 20.90 nm as shown in Figure 3(a) and (b), respectively. On increasing the immersion time to 18 h, interestingly can be observed the Ra and *D* are further increases to 42.33 x 10^2 nm and 22.61 nm as shown in Figure 3(a) and (b), respectively. This happened due to the nucleation growth [31] of CBI crystal structure. Related to the nucleation growth, in which attributed to the mechanism orientation of the CBI hexagonal structure formation that has been discussed in our previous study [7]. Finally, at longer time of immersion, 24 h, surprisingly can be observed that the Ra and *D*, are decreased drastically and accordingly, which proves that there is no more hexagonal side of CBI structure out of the surface compared to what seen earlier in Figure 2(c). This also confirms that the surface of CBI film become smooth and compact as shown in SEM image of Figure 2(e), while the surface roughness

and crystallite size become smaller, whereby the Ra and *D* are 14.38 x 10^2 nm and 15.04 nm as can be observed in Figure 3(a) and (b), respectively. All these explanations also further confirmed that the uniformity and compactness of the CBI film is influenced by Ra and *D* values. Hence, it is expected that the surface roughness will influence the light absorption of CBI film, while the crystallite size expected to influence the CBI cell performance, which will be described further in the UV-Vis section and CBI-PeSCs performance section, respectively. The structural and surface parameters (Ra and *D*) of CBI films are summarized in Table 1.

Table 1
The structural and surface parameters of CBI films at different of immersion times

Immersion times	*D*, (nm)	Ra, (x10^2) (nm)	thickness, *t,* (μm)	E_g (eV)
(a) 1 h	20.76	17.53	0.92	1.81
(b) 6 h	14.50	9.18	1.0	1.82
(c) 12 h	20.90	21.71	2.30	1.98
(d) 18 h	22.61	42.33	2.58	1.67
(e) 24 h	15.04	14.38	4.22	1.65

3.3 UV-vis absorption properties

Figure 4 shows the absorbance spectra of fabricated CBI film and inset indicates the indirect bandgap plotted by Tauc's plot for different immersion times. The UV-Vis absorption test was performed by measuring the transmittance, *T* (λ) and reflectance, *R* (λ) spectra and both variables have been recorded within the wavelength range of 350 – 750 nm. In general, it can be observed that the light absorption is high around 350 nm to 500 nm. It means that the visible region in which is matching with the sunlight spectrum. An increment trend of absorbance intensity changing the immersion times from 1 h to 24 h can be seen in Figure 4, particularly in visible region, however, after around 525 nm at long wavelength region for the sample of 24 h, the light absorption is being slowly dropped in terms of absorbance intensity. It might be due to the thickness of CBI film is thicker which recorded of 4.22 μm as shown in Table 1(e), resulted in less of light absorption and it caused the charge extraction at the active absorber layer become less, particularly at the near-infrared-region (NIR), as shown in Figure 4(e) at 24 h, longer time of immersion. Furthermore, at 1 h of immersion time, the absorbance intensity was low, which is around 0.60 and the band-edge absorption region is 647 nm as can be seen in Figure 4(a). It happened due to the low nucleation growth and crystallization process [7] at shorter of immersion time, as discussed earlier in SEM section, which resulted in defect valley (in yellow colour of SEM image) on the CBI surface and absent of CBI hexagonal shape. However, on increasing the immersion time to 6 h, the absorbance intensity starts to be increased gradually, which is 0.65 and now, its band-edge absorption region is 664 nm as shown in Figure 4(b). Further increasing the immersion time at 12 h, the absorbance intensity increases to around 0. 68 at absorption region of 488 nm due to compact CBI morphology as can be seen in Figure 2(c) and Figure 4(c). This time the band-edge absorption region is extended at 669 nm, which towards the NIR. On prolonging the immersion time to 18 h, interestingly can be observed the absorbance intensity is further increased to 0.75 at the same absorption region of 488 nm, while the band-edge absorption region is extended towards NIR region. It means the light-harvesting is enhanced and the photocurrent increases in the CBI-PeSCs, which means ideal for absorber active layer in a solar cell device. Consequently, more electron produced, and it could probably benefit for the CBI-PeSCs performance. In addition, the light absorption band is higher around the visible region means high

absorption coefficients, hence enhanced the charge transportation and reduces the charge recombination rate [7,21]. As a result, the absorption band is shifted to the long wavelength side compared to other samples, as shown in Figure 4(d). This happened due to a compact morphology and high crystallinity of the CBI film, as discussed previously in the previous SEM and XRD results, respectively, which resulted in a narrower bandgap energy, as shown in Table 1(d) and inset Figure 4, whereby it is expected that will influence the CBI-PeSCs performance, which will be further discussed in CBI-PeSCs performance section.

In this connection, from inset Figure 4 and Table 1, it can be observed that the reduction of optical bandgap (E_g) from 1.81 eV to 1.65 eV as for increased the immersion time from 1 h to 24 h. This reduction is associated with the film thickness of CBI film, which indicates that a compact and high crystallinity film attributed to high light absorption, particularly as shown by sample at 18 h, due to the increased thickness. Therefore, the E_g value of CBI film decreased at longer immersion time, while at shorter immersion time, the E_g increased is due poor film morphology as discussed earlier in SEM images as shown in Figure 2(a) and Table 1(a). This indicates that the ideal film thickness is necessary to obtain optimum optical bandgap when fabricating the CBI films. In addition, at longer time of immersion (24 h), the smaller bandgap is attributed to the small crystallite size as shown in Table 1(e) and Figure 3(b), whereby the reduction in photon scattering from the CBI crystalline grain. Our explanation agrees well with the finding of Ataei *et al.*, who reported that as increasing the thickness of film, the value of optical bandgap (E_g) decreases due to enhanced morphology and crystallinity of the film [31], particularly for the sample at 18 h of immersion times. Eventually, a narrow optical bandgap as shown in our sample gives the advantage for the excitation of an electron from the valence band (VB) state to the conduction band (CB) state as can be seen in inset Figure 4, and it would be beneficial for the charge carrier transport in the active absorber layer of CBI cells device for the charge extraction that will be further discussed in the CBI-PeSCs performance section.

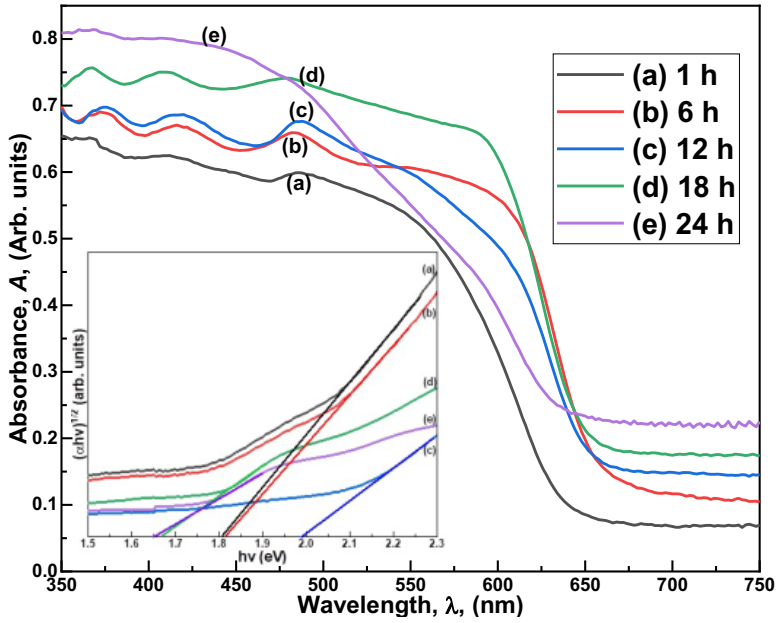

Fig. 4. Absorbance spectra of CBI films at different Immersion times. *Inset* is Tauc's plots of each immersion times

3.4 CBI PeSCs performance

Figure 5 indicates the I-V characteristics of CBI-PeSCs at different immersion times and the inset Figure 5(i) is the image of the fabricated CBI solar cell, while inset Table shows the CBI solar cell

parameters are summarized and its parameters graph is plotted in the Figure 6(a-d). The data measurement in inset Table was taken three times to obtain the average reading of all parameters to ensure the validity of the result, and the measurement was performed in ambient air for four samples. In general, on prolonging the immersion times from 1 h to 24 h, shows that the gradually increment trend of CBI cell performance as can be seen in Figure 6(d), except for sample at 24 h of immersion times, the PCE dropped drastically due to morphology and optical properties, as discussed earlier in SEM and UV section. In brief, the 24 h fabricated sample of CBI produced thicker film contributed to the low absorption light, particularly at the end of band-edge absorption region at 525 nm and onwards as can be observed in Figure 4(e), resulted in poor of charge collectible charge carrier, hence, a charge carrier cannot be transported and collected efficiently, thereby producing a low current density and low voltage as can be seen in Figure 5(e), Figure 6(a) and (b), respectively. According to M. Ataei *et al*., who reported that the improvement in the crystallinity and surface morphology of film contributed to the increment of film thickness [31]. Similarly, an increment of the thickness affects the optical bandgap (E_g), which is the reports showed that the increasing of the thickness resulted in decrement of E_g. Therefore, our result agrees well with this finding, which can be seen in Table 1 (thickness and E_g) and inset Figure 4. It is in line with the XRD and SEM results as discussed earlier. In addition, the increment of the CBI film thickness also attributed to the large crystal size of CBI [7,35] and this crystal grew largely due to the nucleation growth as prolonging the immersion times. It thus affected the produced current density of CBI film at 24 h of longer immersion time, as can be observed in Figure 5(e) and 6(a). Additionally, in the case of longer immersion time, the reason of decrement current density and the device performance is due to small crystallite size of 15.04 nm, as mentioned earlier in Figure 3(b) and UV section. The small *D* size at 24 h of immersion time resulting in the reduction in photon scattering due to the smaller bandgap. Besides, the small crystallite size attributed the high surface area caused the charge carrier cannot be extracted inefficiently at the active absorber layer of CBI cell. As a result, producing a low current and eventually give a poor performance of CBI solar cell device as shown in inset Table of Figure 5, Figure 6(a) and (d), respectively.

On the contrary, at 18 h of immersion times, the optimum value of current density and fill factor are recorded can be seen in Figure 6(a) and (c), respectively. This might be due to the compact and high crystallinity film was fabricated with ideal thickness of CBI film, resulting in large crystallite size of 22.61 nm compared to four other fabricated samples and it thus producing low surface area. As a result, a proper charge carrier can be collected and transported efficiently attributed to the reducing of charge recombination rate. Hence, producing a high current density and voltage as can be observed in Figure 5(d) and inset Table 2 of Figure 5 and, Figure 6(a) and (b) at 18 h, thereby resulting in high percentage of power conversion efficiency as shown in inset Table 2 of Figure 5 and Figure 6(d). In the case of voltage value, the compact morphology with less pinhole-free attributed to 0.12 V at 18 h compared to 1 h, 6 h and 12 h sample. In addition, the rougher surface also contributed to the better device performance, which discussed earlier in SEM section and Figure 3. In brief, the rougher surface of CBI film at 18 h attributed to the less of light scattering as indicated in Table 1(d) and Figure 3(a), whereby reduced the light reflection on the CBI surface through the photon of light is being absorbed and not transmitted out. As a result, the charge recombination decreased in the CBI absorber active layer. Consequently, give a better charge trap and more light harvested, eventually producing a high current density as shown in Figure 6(d) of 18 h.

Furthermore, in the case of 1 h, 6 h and 12 h samples, in general, it can be seen that these three samples shows the trend of increment for the two parameters, which is the fill factor and device performance as shown in Figure 6(c) and (d), respectively, while for the current density and voltage shows increment as well, in Figure 6(a) and (b), except for the sample at 1 h of immersion time due

to poor crystallinity and morphology as discussed earlier in XRD and SEM results, as shown in Figure 1(a) and 2(a) respectively. In brief, poor morphology as shown in SEM images of Figure 2(a) and (b) are created defect of valley and pinhole, which highlighted in yellow and pink colour were contributed to the current leakage, moreover, both CBI films are less rough as shown in Figure 3(a), Table 1(b) and (c) at 6 h and 12 h of immersion times. Corresponding to that, poor charge extraction happened in the absorber layer of CBI-PeSCs attributed to the high charge recombination, thereby producing poor performance of CBI cells as shown in Figure 6(d) and inset Table 2(b) and (c) of Figure 5. In the case of voltage value for three samples were low voltage value due to increasing of the saturation current, J_o, from Eq. (1). However, the poor morphology is mainly caused to the mentioned problem. In addition, a low Ra value for 1 h and 6 h samples are also contributing to low absorption of light as shown in Figure 3(a), which is the reflection of light is high resulted in low absorbance intensity as discussed previously in UV section and it can be seen in Figure 4(a) and (b), compared to sample at 18 h and 24 h. It means the light does not absorb properly, instead the light being reflected or transmitted out of the cell. Thus, poor charge extraction occurred in the absorber layer of CBI, thereby producing a very poor of device performance as shown in Figure 6(d) for the sample at 1 h and 6 h.

$$V_{oc} = \frac{kT}{q} \ln\left(\frac{J_{sc}}{J_o} + 1\right) \quad (1)$$

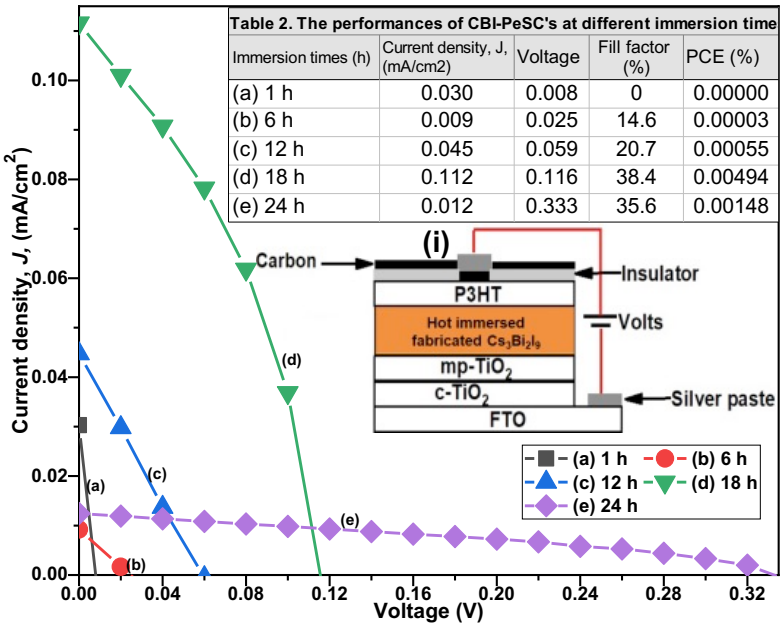

Fig. 5. I-V performance of CBI-PeSCS device at different immersion times using HIM

In this connection, as discussed earlier, a narrow optical bandgap as shown by sample at 18 h and 24 h, gives the advantage for the excitation of an electron from the valence band state to the conduction band state which can quickly generating the collectible charge carriers and thus the charge recombination is decreased at the absorber active layer, thereby producing a better device performance of CBI cell as shown in Figure 6(d) and inset Table 2 of Figure 5. In addition, a compact morphology, less defect and pinhole-free as shown by sample at longer time of immersion (18 h and 24 h) are also contributed to a high voltage value and fill factor as indicated in Figure 6(b) and (c), respectively.

In summary, at the longer of immersion time, a high crystallinity and compact film with a rough surface, smaller crystallite size and pinhole-free, a narrow optical bandgap and ideal film thickness, are identified as three factors that might influences the current density and voltage of CBI-PeSCs at 18 h of immersion time. Eventually, the device performance still showing some improvement, whereby the recorded value of current density and voltage are still attainable by using hot immersion method. However, the obtained value of CBI-PeSCs device performance is still low at present. Therefore, optimum immersion time at 18 h is identified should be explored more with varying the time around 18 h, because it gives hint that the current density and voltage could be improved further. In addition, the challenge in this study such as large crystal structure of CBI (hexagonal shape) and the thickness of the film should be controlled by applying the anti-solvent in HIM approach in the future work. However, this study is not clarified yet and further investigation focusing on HIM with anti-solvent is necessary in the future. The higher efficiency of the state of the art of CBI based perovskite solar cells ever achieved by previous study is 3.20 % [28].

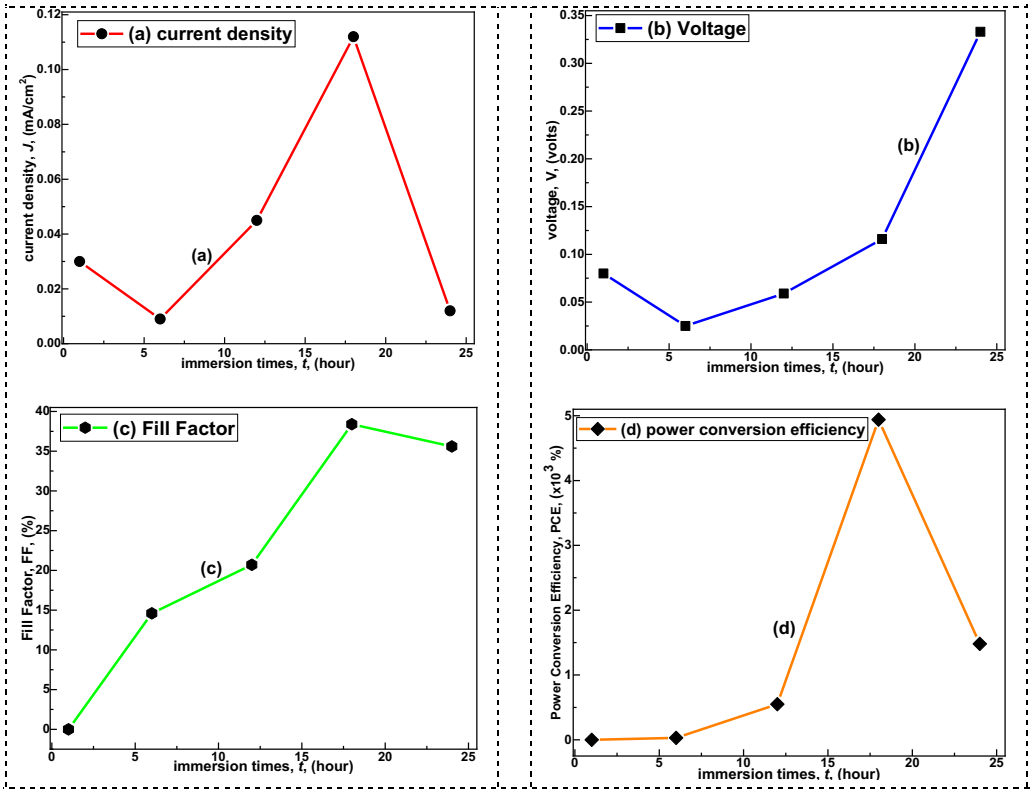

Fig. 6. Solar cell parameters at different immersion times (a) 1 h, (b) 6 h, (c) 12 h, (d) 18 h and (e) 24 h

4. Conclusions

We have successfully fabricated the CBI-PeSCs device and evaluated its performance by changing the immersion times using a simple hot immersion method (HIM), for the first time. The HIM showed that the performance of CBI-PeSCs, particularly the crystallinity, surface morphology, and the absorbance intensity of the CBI film can be enhanced by prolonging the hot immersion time. SEM results showed improved morphology with a compact, uniform, dense and pinhole-free, while smaller crystallite size and rougher film were obtained, as confirmed by the Dektak measurement, which was 22.61 nm and 42.33 x 10^2 nm for the crystallite size and roughness, respectively, while the XRD measurement indicated that the CBI film had a high crystallinity at 18 h of immersion times. UV-

absorption showed that the absorbance intensity increased, and the band-edge absorption region was extended towards NIR wavelength region of 662 nm from 647 nm with a narrower optical bandgap, E_g at 1.67 eV. Eventually, the performance of the CBI-PeSCs device showed fifteen times increment from 0.008 V to 0.12 V for the open-circuit voltage, while the current density showed improvement as well, which was four times increment from 3 x 10^{-2} mA/cm^2 to 0.11 mA/cm^2, resulting in the efficiency of 0.00494% much improved from 0%. Hence, it can be summarized that by changing the immersion times through the hot immersion method, the device performance of CBI solar cells is still achievable, in which relying on the crystallinity, compact film crystallite size, surface roughness, high absorbance intensity and a narrower optical bandgap. Our study gives a new route to fabricating an CBI-PeSCs by HIM to further improve the CBI device performance. Finally, HIM offers a plenty of space to be explored in future to fabricating a Pb-free perovskite solar cells, such as applying the anti-solvent into immersion solution to controlling the crystal size of perovskite structure, study on the effects of volume of immersion solution and varying the thickness of CBI film. Besides, our findings might contribute a new idea to the field of Pb-free PeSCs development, particularly the development CBI based perovskite solar cells.

Acknowledgement
The author would like to acknowledge the Universiti Teknologi MARA (UiTM) for the studies supports, and the authors are grateful for the financial support from the Japanese government and providing the research facilities supports. “This research was not funded by any grant”.

References

[1] Julian Burschka, Norman Pellet, Soo-Jin Moon, Robin Humphry-Baker, Peng Gao, Mohammad K. Nazeeruddin, and Michael Grätzel. “Sequential Deposition as a Route to High-Performance Perovskite-Sensitized Solar Cells.” *Nature* 499, (2013): 316–319. https://doi.org/10.1038/nature12340

[2] Woon Seok Yang, Byung-Wook Park, Eui Hyuk Jung, Nam Joong Jeon, Young Chan Kim, Dong UK Lee, Seong Sik Shin, Jangwon Seo, Eun Kyu Kim, Jun Hong Noh, and Sang IL Seok. “Iodide management in formamidinium-lead-halide-based perovskite layers for efficient solar cells.” *Science* 356, no. 6345 (2017): 1376–1379. https://doi:10.1126/science.aan2301

[3] Lee Sang-Won, Kim Seongtak, Bae Soohyun, Cho Kyungjin, Chung Taewon, Mundt Laura E, Lee Seunghun, Park Sungeun, Park Hyomin, Schubert Martin C, Glunz Stefan W, Ko Yohan, Jun Yongseok, Kang Yoonmook, Lee Hae-Seok, and Kim Donghwan. “UV degradation and recovery of perovskite solar cells.” *Science Reports* 6, (2016): 38150. https://doi.org/10.1038/srep38150

[4] Rhrissi Ilyass, El Harafi O, Arba Youssef, and Moubah, Reda. “Impact of film thickness on the structural and linear/nonlinear optical properties in highly oriented $Cs_3Bi_2I_9$ perovskite films.” *Materials Science Engineering B* 297, (2023): 116784. https://doi:10.1016/j.mseb.2023.116784

[5] Michael Kulbak, David Cahen, and Gary Hodes. “How improtant is the organic part of lead halide perovskite phitiovoltaic cells? efficient $CsPbBr_3$ cells.” *Journal of Physical Chemistry Letters* 6, no. 13 (2015): 2452–2456. https://doi.org/10.1021/acs.jpclett.5b00968

[6] Lyu Miaoqiang, Yun Jung-ho, Cai Molang, Jiao Yalong, Bernhardt Paul V, Zhang Meng, Wang Qiong, Du Aijun, Wang Hongxia, Liu Gang, and Wang Lianzhou. “Organic – inorganic bismuth (III)-based material: A lead-free, air-stable and solution-processable light-absorber beyond organolead perovskites.” *Nano Research* 9, (2016): 692–702. https://doi.org/10.1007/s12274-015-0948-y

[7] Achoi Mohd Faizal, Kato Shinya, Kishi Naoki, and Soga Tetsuo. “Improved photovoltaic properties of $((CH_3NH_3)_{1-x}Cs_x)_3Bi_2I_9$: (x = 0-1.0) hybrid perovskite solar cells via a hot immersion method.” *AIMS Materials Science* 11, (2024): 605–619. https://doi.org/10.3934/matersci.2024031

[8] Shahiduzzaman Md, Hossain Mohammad Ismail, Gantumur Munkhtuul, Yue Feng, Rafij Junayed Hossain, Akhtaruzzaman Md, Nakano Masahiro, Karakawa Makoto, Tomita Koji, Nunzi Jean Michel, and Taima Tetsuya. “Unlocking high stability in perovskite solar cells through vacuum-deposited $Cs_3Bi_2I_9$ thin layer.” *Nano Energy* 127, (2024): 109726. https://doi.org/10.1016/j.nanoen.2024.109726

[9] Yoo Jason J, Seo Gabkyung, Chua Matthew R, Park Tae Gwan, Lu Yongli, Rotermund Fabian, Kim Young-Ki, Moon Chan Su, Jeon Nam Joong, Correa-Baena, Juan-Pablo, Bulović Vladimir, Shin Seong Sik, Bawendi Moungi G, and Seo

Jangwon. "Efficient perovskite solar cells via improved carrier management." *Nature* 590, (2021): 587–593. https://doi.org/10.1038/s41586-021-03285-w

[10] McClure Eric T, Ball Molly R, Windl Wolfgang, and Woodward Patrick M. "Cs_2AgBiX_6 (X: Br, Cl): New Visible Light Absorbing, Lead-Free Halide Perovskite Semiconductors." *Chemistry of Materials* 28, no. 5 (2016): 1348-1354. https://doi.org/10.1021/acs.chemmater.5b04231

[11] Eperon Giles E, Stranks Samuel D, Menelaou Christopher, Johnston Michael B, Herz Laura M, and Snaith Henry J. "Formamidinium lead trihalide: A broadly tunable perovskite for efficient planar heterojunction solar cells." *Energy Environmental Science* 7, (2014): 982–988. https://doi.org/10.1039/c3ee43822h

[12] Riley E. Brandt, Vladan Stevanovic, David S. Ginley, and Tonio Buonassisi. "Identifying defect-tolerant semiconductors with high minority-carrierlifetimes beyond hybrid lead halide perovskites." *MRS Communications* 5, (2015): 265–275. https://doi.org/10.1557/mrc.2015.26

[13] Devasia Sebin, Shaji Sadasivan, Avellaneda David Avellaneda, Aguilar Martinez, Josue Amilcar, and Krishnan Bindu. "In situ grown Bi_2S_3 nanorods in $Cs_3Bi_2I_9$ thin films as broadband self-driven photodetector with improved photostability." *Optical Materials (Amst)* 152, (2024): 115532. https://doi.org/10.1016/j.optmat.2024.115532

[14] Dong Kailian, Zhou Hai, Xiao Meng, Gui Pengbin, Gao Zheng, Yao Fang, Shao Wenlong, Liu Chenwei, Tao Chen, Ke Weijun, and Fang Guojia. "Semi-transparent, high-performance lead-free $Cs_3Bi_2I_9$ single crystal self-driven photodetector. *Applied Physical Letter* 120, (2022): 191102. https://doi.org/10.1063/5.0090569

[15] Li Luji, Ye Gang, Luo Tianyuan, Chen Xiayan, Zhang Gaojie, Wu Hao, Yang Li, Zhang Wenfeng, and Chang Haixin. "Centimeter-Sized Stable Zero-Dimensional $Cs_3Bi_2I_9$ Single Crystal for Mid-Infrared Lead-Free Perovskite Photodetector." *Journal of Physical Chemistry C* 126, (2022): 3646–3652. https://doi.org/10.1021/acs.jpcc.1c08815

[16] Li Ziqing, Liu Xinya, Zuo Chaolei, Yang Wei, and Fang Xiaosheng. "Supersaturation-Controlled Growth of Monolithically Integrated Lead-Free Halide Perovskite Single-Crystalline Thin Film for High-Sensitivity Photodetectors." *Advance Materials* 33, no. 41 (2021): 2103010. https://doi.org/10.1002/adma.202103010

[17] Sanders Stephen, Stümmler Dominik, Pfeiffer Pascal, Ackermann Nils, Simkus Gintautas, Heuken Michael, Baumann Peter K, Vescan Andrei, and Kalisch Holger. "Chemical Vapor Deposition of Organic-Inorganic Bismuth-Based Perovskite Films for Solar Cell Application." *Science Reports* 9, no. 1 (2019): 9774. https://doi.org/10.1038/s41598-019-46199-4

[18] Aiba Shunsuke, Achoi Mohd Faizal, Kato Shinya, Kishi Naoki, and Soga Tetsuo. "Influence of Anti-Solvents on the Performance of Cesium Bismuth Iodide Perovskite Solar Cells." *Key Engineering Material* 951, (2023): 105–114. https://doi.org/10.4028/p-mv5QXw

[19] Mutlu Adem, Yesil Tamer, and Zafer Ceylan. "Utilization of coordinating green solvents for high quality methylammonium bismuth iodide thin films for photovoltaic applications." *Organic Electronics* 95, (2021): 106191. https://doi.org/10.1016/j.orgel.2021.106191

[20] Achoi Mohd Faizal, Aiba Shunsuke, Kato Shinya, Kishi Naoki, and Soga Tetsuo. "A novel approach towards compact and improved-crystallinity methylammonium bismuth iodide film via hot immersion method." *Materials Letter X* 16, (2021): 100096. https://doi.org/10.1016/j.mlblux.2021.100096

[21] Achoi Mohd Faizal, Kato Shinya, Kishi Naoki, and Soga Tetsuo. "Annealing Time Dependence in the Fabrication of Bismuth-based Perovskite Solar Cells (Bi-PeSCs) by the Hot Immersion Method." *Journal of Mechanical Engineering* 21, (2024): 83–103. https://doi.org/10.24191/jmeche.v21i1.25361

[22] Achoi Mohd Faizal, Aiba Shunsuke, Kato Shinya, Kishi Naoki, and Soga Tetsuo. "Influence of Post-Annealing on the Properties of Methylammonium Bismuth Iodide Perovskite Solar Cells Through the Hot Immersion Method." *Journal of Electronic Materials* 52, (2023): 351–367. https://doi.org/10.1007/s11664-022-09994-w

[23] Ben Bechir Mohamed and Alresheedi Faisal. "Electrical and optical investigations lead-free Cesium Bismuth iodide single crystal." *Optical Materials (Amst).* 147, (2024): 114621. https://doi.org/10.1016/j.optmat.2023.114621

[24] Shargaieva Oleksandra, Lang Felix, Rappich Joerg, Dittrich Thomas, Klaus Manuela, Meixner Matthias, Genzel Christoph, and Nickel Norbert H. "The influence of the grain size on the properties of $CH_3NH_3PbI_2$ thin films." *ACS Applied Material Interfaces* 9, (2017): 38428–38435. https://doi.org/10.1021/acsami.7b10056

[25] Mohd Faizal Achoi, Shunsuke Aiba, Shinya Kato, Naoki Kishi, and Tetsuo Soga. "A novel approach towards compact and improved-crystallinity methylammonium bismuth iodide film via hot immersion method." *Materials Letters: X* 16, (2021): 100096. https://doi.org/10.1016/j.mlblux.2021.100096

[26] Mohd Faizal Achoi, Shunsuke Aiba, Shinya Kato, Naoki Kishi, and Tetsuo Soga. "Effect of spinning rate on the performance of multilayer Bi-perovskite solar cells." *International Journal Nanoelectronics Materials* 14, (2021): 1–10. https://ijneam.unimap.edu.my/images/PDF/InCAPE2021/Vol_14_SI_Dec_2021_1-10.pdf

[27] Matiur Rahman Md, Kato Shinya, and Soga Tetsuo. "All-solution-processed environment-friendly solid-state BiOI photovoltaic cell with high-short-circuit current by successive ionic layer adsorption and reaction (SILAR)." *Journal of Materials Science: Materials in Electronics* 32, (2021): 18342–18350. https://doi.org/10.1007/s10854-021-

06375-7

[28] Trilok Singh, Ashish Kulkarni, Masashi Ikegami, and Tsutomu Miyasaka. "Effect of electron transporting layer on bismuth-based lead-free perovskite $(CH_3NH_3)_3Bi_2I_9$ for photovoltaic applications." *ACS Applied Materials and Interfaces* 8, no. 23 (2016): 14542–14547. https://doi.org/10.1021/acsami.6b02843

[29] Mutalifu Abulikemu, Samy Ould-Chikh, Xiaohe Miao, Erkki Alarousu, Banavoth Murali, Guy Olivier, Ngongang Ndjawa, Jeremy Barbé, Abdulrahman El Labban, Aram Amassian, and Silvano Del Gobbo. "Optoelectronic and photovoltaic properties of the air-stable organohalide semiconductor $(CH_3NH_3)_3Bi_2I_9$." *Journal Materials Chemistry A* 4, no. 32 (2016): 12504–12515. https://doi.org/10.1039/C6TA04657F

[30] Zhijie Ma, Sun Peng, Yihui Wu, Xiang Fang, Xin Chen, Xuguang Jia, Kezhi Zhang, Ningyi Yuan, Jianning Ding, and Ning Dai. "Air-stable layered bismuth-based perovskite-like materials: structures and semiconductor properties." *Physica B: Condensed Matter* 526, (2017): 136–142. https://doi.org/10.1016/j.physb.2017.08.079

[31] Mohammad Ataei, Mehdi Adelifard, and Seyed Saeid Hosseini. "Physical properties and photovoltaic performance of perovskite solar cells based on lead-free $A_3Bi_2I_9$ (A = CH_3NH_3, Cs) active layers." *Journal of Electronic Materials* 50, (2021): 571–579. https://doi.org/10.1007/s11664-020-08580-2

[32] Yasuhiro Shirahata. "Effects of annealing temperature on photovoltaic properties of lead-free $(CH_3NH_3)_3Bi_2I_9$ solar cells." *Journal of the Ceramic Society Japan* 128, no. 5 (2020): 298–303. https://doi.org/10.2109/jcersj2.19156

[33] Zhang Hongjian, Xu Yadong, Sun Qihao, Dong Jiangpeng, Lu Yufei, Zhang Binbin, and Jie Wangi. "Lead free halide perovskite $Cs_3Bi_2I_9$ bulk crystals grown by a low temperature solution method." *Cystal Engineering Communications* 20, (2018): 4935–4941. https://doi.org/10.1039/C8CE00925B

[34] Dhruba B. Khadka, Yasuhiro Shirai, Masatoshi Yanagida, and Kenjiro Miyano. "Tailoring the film morphology and interface band offset of caesium bismuth iodide-based Pb-free perovskite solar cells." *Journal of Materials Chemistry C* 7, no. 27 (2019): 8335–8343. https://doi.org/10.1039/C9TC02181G

[35] Achoi Mohd Faizal, Kato Shinya, Kishi Naoki, and Soga Tetsuo. "Properties of $((CH_3NH_3)_{1-x}Cs_x)_3Bi_2I_9$: (x=0-1.0) Hybrid Perovskite Solar Cells with Chlorobenzene Treatment." *Journal of Solar Energy Research Update* 11, (2024): 37–44. https://www.zealpress.com/jms/index.php/jseru/article/view/566

[36] Xiao Zhengguo, Bi Cheng, Shao Yuchuan, Dong Qingfeng, Wang Qi, Yuan Yongbo, Wang Chenggong, Gao Yongli, and Huang Jinsong. "Efficient, high yield perovskite photovoltaic devices grown by interdiffusion of solution-processed precursor stacking layers." *Energy Environmental Science* 7, (2014): 2619–2623. https://doi.org/10.1039/c4ee01138d

[37] Masawa Salma Maneno, Li Jihong, Zhao Chenxu, Liu Xiaolong, and Yao Jianxi. "0D/2D Mixed Dimensional Lead-Free Caesium Bismuth Iodide Perovskite for Solar Cell Application." *Materials (Basel)* 15, (2022): 2180. https://doi.org/10.3390/ma15062180